Anal Bioanal Chem (2009) 394:399–411
DOI 10.1007/s00216-009-2614-2

ORIGINAL PAPER

Estimation of surface desorption times in hydrophobically coated nanochannels and their effect on shear-driven and pressure-driven chromatography

Frederik Detobel · Veronika Fekete · Wim De Malsche · Selm De Bruyne · Han Gardeniers · Gert Desmet

Received: 23 October 2008 / Revised: 7 January 2009 / Accepted: 9 January 2009 / Published online: 13 February 2009

Abstract The present paper provides a detailed analysis of the analyte-wall adsorption effects in nanochannels, including a random walk study of the analyte-wall collision frequency, and uses these insights to estimate wall desorption times from chromatographic experiments in nanochannels. Using coumarin dye analytes and using a methanol/water mixture buffered at pH 3 in 120-nm deep channels, the surface desorption times on naked fused-silica glass were found to be maximally of the order of 60 to 150 μs, while they were found to be on the order of 100 to 500 μs on a hydrophobically coated wall. These nonzero adsorption and desorption times lead to an additional band broadening when conducting chromatographic separations. Shear-driven flows, requiring a noncoated moving wall and a stationary coated wall, intrinsically turn out to be more prone to this effect than pressure-driven or electro-driven flows for example. The present study also shows that, interestingly, the number of analyte-wall collisions increases with the inverse of the channel depth and not with its second power, as would be expected from the Einstein–Smoluchowski relationship for molecular diffusion.

Keywords Shear-driven chromatography · Analyte-wall collisions · Band broadening · Random walk simulations

F. Detobel · V. Fekete · W. De Malsche · S. De Bruyne · G. Desmet (✉)
Department of Chemical Engineering, Vrije Universiteit Brussel, 1050 Brussels, Belgium
e-mail: gedesmet@vub.ac.be

H. Gardeniers
Research Program Mesofluidics, MESA+ Institute for Nanotechnology, 7500 Enschede, The Netherlands

Abbreviations

CE	Capillary electrophoresis
CEC	Capillary electrochromatography
ED	Electro-driven
EM CCD	Electron multiplying charge-coupled device
LC	Liquid chromatography
LPCVD	Low-pressure chemical vapor deposition
OT	Open-tubular
PD	Pressure-driven
RIE	Reactive ion etching
SD	Shear-driven
SDC	Shear-driven chromatography

Introduction

The past years have shown a clear trend towards the exploration of ever smaller channels in the microfluidics and the lab-on-a-chip field [1–8]. One of the fundamental implications of this pursued miniaturization is the overwhelming increase in the number of analyte-wall collisions. To the best of our knowledge, surprisingly little literature resources are available to estimate exactly how large this number is. Nor is there much literature available about the finite time needed for the adsorption and desorption events occurring at the wall [9]. This finite time arises from the fact that molecules, once adsorbed on the wall, need to surmount a certain (activation) energy barrier before they can (abruptly) leave the surface [10]. Although this desorption time may be either very short or very long (depending upon the nature of the physical or chemical bond between the analytes and the wall surface), it can be inferred that, in the case of nanochannels, the total time a molecule spends in an adsorbed state will always represent

an important fraction of the mean residence time, given the large number of analyte-wall collisions. Apart from more practical problems such as channel fouling, this nonzero contact time can also lead to a fundamental deterioration of the separation power if such channels are used to conduct open-tubular capillary electrophoresis (CE) or liquid chromatography (LC).

We stumbled upon this problem by performing high-speed reversed-phase chromatography separations using shear-driven flows through nanochannels (operating principle, see Fig. 1b) and noting that peaks with a large retention coefficient yielded a band broadening that was larger than theoretically expected. In most of the past shear-driven chromatography (SDC) experiments conducted in our group [11–15], the emphasis was on separations of molecules having a small retention coefficient (mainly because the linearly moving wall was too short to bring a strongly retained species far enough in the channel to establish separation). When trying to increase the retention factor (by switching to mobile phases that are less hydrophilic), we however experienced great difficulties in obtaining plate height values that were close enough to the theoretically expected value. The present contribution provides an account of our efforts to elucidate this problem.

The observed additional band broadening (clearly depending on the chromatographic retention coefficient k' of the species) was initially attributed to microscopic heterogeneities of the stationary phase monolayer that was deposited on the wall [14] (and this contribution can still not be entirely excluded), but basic calculations based on some literature values for wall adsorption times show that the finite adsorption/desorption time might very well contribute to an increased band broadening.

Giddings' adsorption/desorption theory

The basic foundations for this additional band broadening, further referred to as H_{ads}, have been laid out by Giddings, already back in 1965 [10]. He showed that, in cases with large desorption times, this H_{ads} contribution should be added to the "normal" plate height value, which, in open-tubular liquid chromatography, only accounts for the longitudinal diffusion and the mobile-phase mass transfer (related to the time needed to sample all the different velocity lines in the mobile phase zone), such that:

$$H = \frac{2D_M}{u_m} + 2C_m u_m \quad (1)$$

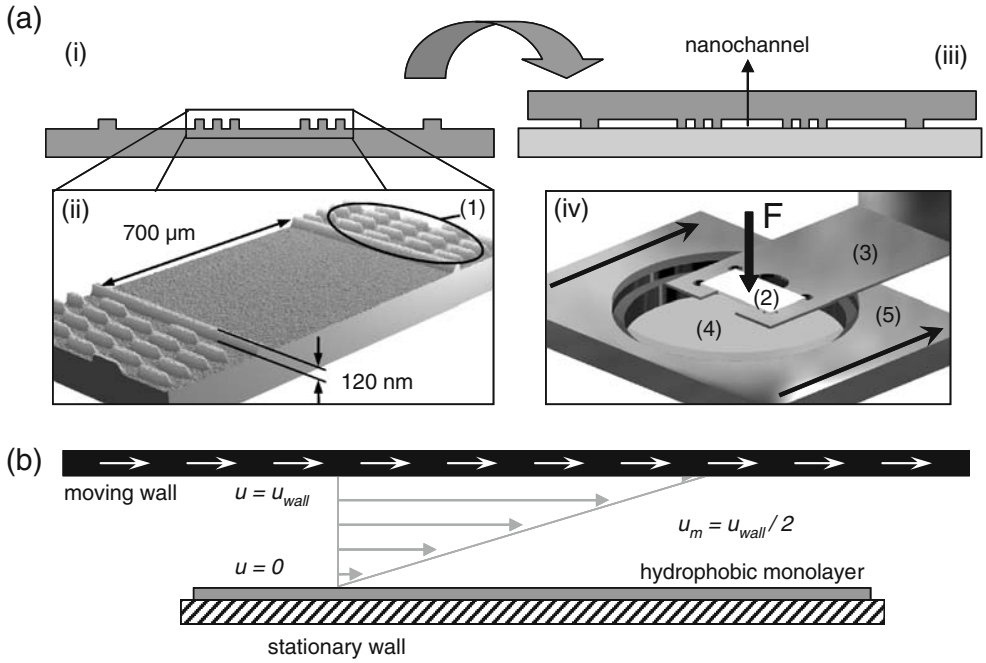

Fig. 1 **a** Schematic overview of the different parts for shear-driven nanochannel assembly. *(i)* Cross-sectional schematic view of the stationary wall with etched micropattern. *(ii)* Noncontact optical profiler image of the microstructured spacer regions *(1)* defining the channel dimensions. *(iii)* The patterned stationary wall is placed upside-down on top of a second flat fused silica substrate. *(iv)* Assembly of the nanochannel for shear-driven chromatography. The stationary wall *(2)* is immobilized using a stationary holder *(3)* and pushed (with force *F*) onto the flat fused silica substrate *(4)*. This fused-silica substrate is moved in the axial direction of the nanochannel (*direction of the arrows*) by means of a holder *(5)* connected to a linear translation stage (not shown). **b** Schematic longitudinal cross-section of a rectangular channel illustrating the shear-driven flow and chromatography principle. The movement of one channel wall relative to the opposite one generates a flow through the channel based on viscous drag forces [25]. The hydropobic coating on the stationary wall induces the chromatographic separation

Wherein H is the plate height, D_M is the molecular diffusion coefficient of the analyte, and u_m is the linear mobile phase velocity. C_m is a measure for the mass transfer resistance in the mobile phase and depends on the applied flow mechanism and the chromatographic retention factor k', usually defined via the ratio of the actual velocity (u_r) of a migrating band versus the velocity of a band of nonretained species, migrating at the linear mobile phase velocity (u_m) in case of a stationary phase monolayer:

$$k' = \frac{u_m}{u_r} - 1 \tag{2}$$

Typical expressions for C_m are given in Table 1.

According to Giddings, the shortcoming of Eq. 1 is that it is based on the assumption that the time spent on the monolayer surface is negligibly small. However, if the desorption takes a finite time, an extra term needs to be added, which, according to Giddings, can be calculated as [10]:

$$H_{ads} = 2\frac{k'}{(1+k')^2} u_m t_d \tag{3}$$

wherein k' is the retention factor, u_m is the mobile phase velocity, and t_d is the mean time a molecule spends on the stationary phase before it desorbs from it. The expression in Eq. 3 should be considered as the equivalent of the so-called stationary phase mass transfer term (C_s term [10, 16]), that is typically added to Eq. 1 if the stationary phase in the open tube or channel is a porous layer with a finite thickness [17]. In the case of a monolayer coating (as is the case in the presently considered systems), this term is usually neglected because there is no time needed to diffuse across a given thickness of porous layer material. However, going to the extreme detail, there is still a finite time associated with the process of adsorption and desorption at and from this monolayer. This finite time then gives rise to an additional type of band broadening, represented by Eq. 3.

Obviously, t_d is a crucial parameter in this equation (H_{ads} tends to zero if t_d becomes infinitely small). Clearly, the value of t_d greatly depends upon the nature of the analytes and the wall surface. The values for t_d that can be found in literature are hence very widespread, from the microsecond range [9] over the millisecond range [18], up to a few hundred or thousands of milliseconds [19, 20] and extending even into the minute range [21]. Considering now that a recent study reported a typical liquid-phase desorption time of 2 ms for acetophenone and hydroquinone on a C18-coated silica surface [18] and using this value in Eq. 3, the additional band broadening due to the finite adsorption–desorption time can be expected to be of the order of 1.8 μm for typical values of k'=2 and u_m=2 mm/s. This H_{ads} value is much larger than the typical plate height values of about H=0.3 μm that are predicted by Eq. 1 and the first equation (T1) from Table 1 for k'=2 and u_m= 2 mm/s if there would be no finite desorption time contribution. It therefore certainly needs to be investigated whether the unusually high plate height values that were measured when conducting separations at high k' cannot be explained by the H_{ads} contribution.

Overview of the present study

In the first paragraph of "Experimental observations," the experimental plate height values derived under both low and high retentive conditions in a chromatographic shear-driven nanochannel are presented and compared with the theoretically expected value when the additional band broadening by finite desorption time effects is neglected. By assuming that the difference between the theoretical and experimental plate height values is completely caused by these adsorption/desorption effects, one should be able to make an estimation of the desorption times of the analytes on the different channel walls. Therefore, a generalized theoretical plate height expression is established, based on Giddings' random walk theory, which relates the additional band broadening due to adsorption/desorption effects in shear-driven chromatographic channels to the desorption time values ("Establishment of a theoretical plate height expression").

Table 1 Expressions for C_m and H_{ads} for the case of pressure-driven LC, electro-driven CEC and CE and shear-driven LC in open-tubular channels with flat-rectangular cross section

Label of equation		Equation	Reference
OT-PD	(T1)	$C_m = \frac{1}{210}\cdot\frac{1+9k'+\frac{51}{2}k'^2}{(1+k')^2}\cdot\frac{d^2}{D_M}$	[29]
CE	(T2)	C_m=0	[30]
OT-CEC	(T3)	$C_m = \frac{1}{6}\cdot\frac{k'^2}{(1+k')^2}\cdot\frac{d^2}{D_M}$	[31]
OT-SD	(T4)	$C_m = \frac{1}{30}\cdot\frac{1+7k'+16k'^2}{(1+k')^2}\cdot\frac{d^2}{D_M}$	[25]
OT-PD	(T5)	$H_{ads} = 2\frac{k'}{(1+k')^2}u_m t_d$	[10]
CE OT-CEC OT-SD	(T6)	$H_{ads,SD} = \frac{u_m}{(k'+1)^2}A$ with $A = \frac{\left(3k'^2t_c^2+(2k'+1)^2t_{g1}^2+2k'(2k'+1)t_c t_{g1}\right)}{\left(t_c+t_{g1}\right)}$	Present study

However, to be able to calculate the desorption times from this equation, the mean time between two collisions of the analyte with either wall of the nanochannel should be known. By means of a random walk analysis in 1-D and 3-D, a second expression is established for this mean collision time ("General expression for t_c derived from random walk simulations" in "Determination of mean time t_c between two subsequent collisions with a wall") which is further related to the physico-chemical parameters of the analyte using Langevin's theory of Brownian motion ("Explicit expression for t_c using Langevin's theory" in "Determination of mean time t_c between two subsequent collisions with a wall"). Based on the different derived expressions, the desorption times of the analytes on a nontreated and a hydrophobically coated fused silica substrate were calculated, and their implication on the chromatographic performance of open-tubular nanochannels is discussed ("Extraction of the mean adsorption–desorption times from the experimental data and their implication on the chromatographic performance of open-tubular nanochannels").

The emphasis of the present study is on channels carrying a hydrophobic monolayer coating of alkyl chains, for this is the coating that is typically used in reversed-phase liquid chromatography, in turn the most frequently employed form of liquid chromatography. In the present case, a C12 monolayer was used as this coating displayed a better channel-to-channel repeatability than a C18 monolayer while still providing a sufficiently large retention capacity.

In hindsight, it should not have come as a surprise that finite desorption time effects are bound to show up during shear-driven flow experiments in nanometric deep channels because the effect is proportional to u_m (see Eq. 3), and shear-driven flows allow the establishment of very high velocities (even in nanochannels), while apparently (see "Conclusion" section) the specific geometry of a shear-driven flow system is more sensitive to effects of nonzero desorption times than an electro- or a pressure-driven flow system.

Materials and methods

Chemicals and samples

Coumarin 450 (C450, CAS no. 26078-25-1), coumarin 460 (C460, CAS no. 91-44-1), and coumarin 480 (C480, CAS no.41267-76-9) were purchased from ACROS (Geel, Belgium). The coumarins were dissolved in a 70:30% and 50:50% (*v*/*v*) mixture of methanol (high-performance LC grade) and 10 mM phosphate buffer (pH 3), used as the mobile phase for two separation experiments. The separation surface (bottom wall of the open nanochannel trenches) was coated with a monolayer of dimethyl-dodecyl-chlorosilane (C12, CAS no. 66604-31-7) following the protocol described in [14].

Nanochannel fabrication and experimental setup

The nanochannels were microfabricated in a fused-silica wafer (0.5 mm thick and with a diameter of 4 in., Virginia Semiconductor Inc.). First, mid-UV lithography was used to define the spacers in a positive resist layer with a thickness of 1.2 μm, deposited on the wafer surface. Next, the pattern was transferred into the fused silica by reactive ion etching (Adixen Alcatel AMS100DE). Finally, the resist was removed by nitric acid and oxygen plasma. Fig. 1a gives a close view of the etched pattern, defining the channel dimensions. The channel side walls are formed by two spacers, 120 nm in height and placed 700 μm apart. During the experiments, the platelets carrying the spacers were kept stationary and pushed (by applying a normal load pressure of 1 bar using a pneumatic cylinder) onto a second flat round fused-silica substrate (Photox Optical Systems, Sheffield, UK) to maintain a good contact between the spacers and this second fused-silica substrate (Fig. 1a). The latter, having a flatness of $\lambda/10$ per inch at λ=632.8 nm (i.e., the standard measuring conditions), serves as the moving wall for the shear-driven flow generation (Fig. 1b). To reduce the friction between the spacers and the second fused-silica substrate, microstructures were patterned inside the spacer region (Fig. 1a). The roughness of the channel walls was determined using a noncontact optical profiler (Wyko®, Veeco Instruments BV). The remainder of the setup (both the mechanical and the optical parts) as well as the procedures adopted to inject the samples have already been described elsewhere [14, 15].

Determination of chromatographic parameters

Two cases of SDC have been considered: one using strong retention conditions (50:50% (*v*/*v*) methanol/water) and one with weak retention conditions (solvent with a higher hydrophobicity, 70:30% (*v*/*v*) methanol/water). In both cases, the aqueous solution was buffered to pH=3 to reduce ion-exchange interactions of the coumarins with the residual silanols, as these groups can act as strong adsorption sites for organic cations (such as the presently considered coumarins) and cause tailing of the peaks [20, 21]. Each velocity was repeated at least four times. After each run, both the moving wall and the stationary wall were abundantly rinsed with the mobile phase.

Similar to the procedures described in [12, 14], the wall movement was stopped abruptly after having elapsed a given distance (between 3 and 8 mm in the present case). This was needed to record the coumarin dye peaks with a

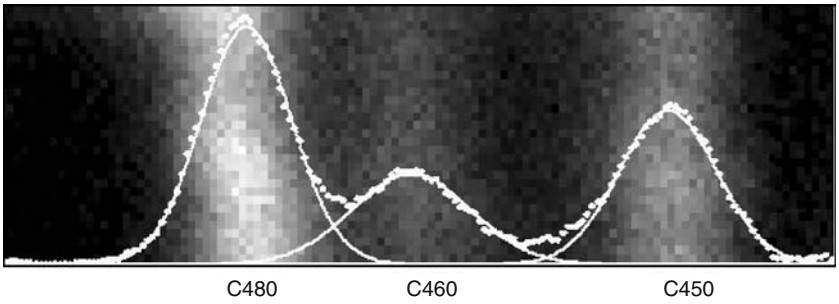

Fig. 2 Typical EM CCD image of a SDC separation of three fluorescent coumarin dyes (c450, c460, and c480) in a 120-nm deep channel under strong retention conditions (50:50% (*v*/*v*) methanol/H_2O). The corresponding fluorescence intensity curve, presented as *white dots overlaying the image*, was used to calculate the variances of the different peaks by fitting the experimental data points with a Gaussian curve (*full lines*)

sufficiently high spatial resolution and S/N ratio because the peaks move so fast that "on-the-fly" measurements of the peak shape were impossible. The detection of the coumarin peaks was performed using an inverted microscope connected to an electron multiplying charge-coupled device (EM CCD) camera (ImageEMC9100-13, Hamamatsu Photonics, Louvain-la-Neuve, Belgium), working at a frame rate of 100 frames per second and operated in "binning 2"-mode, implying a pixel size of 7 μm. The still camera images were analyzed using the Wasabi Hamamatsu software accompanying the employed EM CCD camera. This allowed the automatic read-out of the intensity of each pixel and the storage of this information in an Excel file. From this file, it was straightforward to reconstruct the peak intensity profiles. The retention factor k' of the sample components was calculated from the difference between the virtual position L_0 of the nonretained mobile phase liquid (moving with exactly one half of the moving wall velocity), and the actual position L_{eff} of the peak maximum of one of the retained components, using [13]

$$k' = \frac{L_0 - L_{\mathrm{eff}}}{L_{\mathrm{eff}}} \tag{4}$$

The band broadening was quantified using the SigmaPlot software package (Systat Software, Richmond, CA, USA) to fit the peak intensity profiles with a Gaussian curve function, directly yielding a value for the spatial peak variance σ^2. Using the definition of the plate height, the thus obtained variances were translated into experimental plate height values H_{meas}:

$$H_{\mathrm{meas}} = \frac{\sigma^2}{L_{\mathrm{eff}}} \tag{5}$$

The diffusion coefficient values needed to calculate the theoretically predicted plate heights via Eq. 1 and (T4) from Table 1 were determined using the Wilke–Chang calculation described in [22]. For the 50:50% (*v*/*v*) methanol/water mixture, the diffusion coefficient D_{M} was calculated to be 3.5×10^{-10}, 3.2×10^{-10}, and 3.1×10^{-10} $m^2\ s^{-1}$ for coumarin C450, C460, and C480, respectively, at a temperature of 293 K. For the 70:30% (*v*/*v*) methanol/water mixture, values of 4.1×10^{-10}, 3.8×10^{-10}, and 3.7×10^{-10} $m^2\ s^{-1}$ were found.

Results and discussion

Experimental observations

A typical chromatogram obtained after the separation of the mixture of three coumarins under the strong retention conditions is given in Fig. 2. The C460 component has a lower quantum yield and therefore always yielded a lower signal. Under low-retention conditions, the peaks were shaper and better separated (data not shown). The variances of the different peaks were then determined by fitting the experimental data points belonging to the different peaks with a Gaussian curve (full lines). These variances were subsequently transformed into the experimental plate height values (H_{meas}) using Eq. 5.

Figure 3 shows a plot of the plate height values H', obtained after correcting the measured plate height values by subtracting the contribution from the injection peak width ($H_{\mathrm{inj}}=w_{\mathrm{inj}}^2/12L$ [23]) and the theoretically expected plate height:

$$H' = H_{\mathrm{meas}} - \frac{w_{\mathrm{inj}}^2}{12L} - H_{\mathrm{theo}} \tag{6}$$

Wherein w_{inj} was taken equal to 100 μm, the preset injection width, and wherein H_{theo} is obtained by Eq. 1 and (T4) from Table 1. Typically, H_{theo} is of the order of 0.2 μm, and $w_{\mathrm{inj}}^2/12L$ was of the order of 0.4 μm.

As can be noted from Fig. 3, the scatter on the H' data is fairly large. This scatter reflects the rather large measurement uncertainty we experienced. A given part of this scatter was certainly due to the relatively low S/N ratio of the recorded peaks and the associated peak width determi-

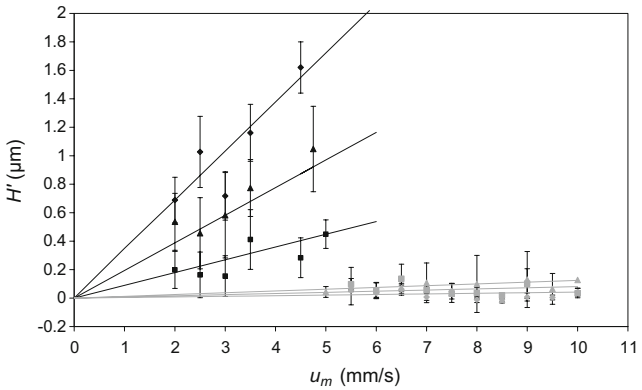

Fig. 3 Plot of H' versus u_m (see Eq. 6 for definition of H') for C450 (*closed rectangles*), C460 (*closed triangles*) and C480 (*closed diamonds*) for the strong retention case (*black data points*) and for the weak retention case (*gray data points*). The *full lines* represent the best linear fit (with intercept=0). The *error bars* represent the standard deviation obtained from at least four repeats per tested velocity

nation problems, despite the use of a state-of-the-art EM CCD camera, capable of detecting low fluorescent signals while maintaining a high quantum efficiency. The major part of the scatter however appeared to be inherent to the physico-chemistry of the studied system. It was observed that successive repeats of the experiment typically gave a plate height value that fluctuated with some 0.2 to 0.5 µm. This large scatter was typical under high retention conditions, whereas the scatter on data obtained in the low retention case was much smaller, so that it seems unlikely that the scatter is related to measurement errors or mechanical or optical setup problems. We therefore believe these fluctuations are due to differences in adsorbed species that are remnants of a previous run, despite the use of abundant amounts of fresh mobile phase to clean the wall surfaces between successive runs.

Despite the large scatter, Fig. 3 clearly shows that the weak retention case (leading to small retention factors of k'=0.07; 0.15 and 0.2, for coumarin C450, C460, and C480, respectively) only yields a very small deviation from the theoretical expectation (even negative H' values are observed), whereas the strong retention case (leading to larger retention factors: k'=0.29, 0.69, and 1.10 for coumarin C450, C460, and C480, respectively) leads to a significant excess plate height value. This value appears to increase with the velocity, in agreement with Eq. 3, and hence suggesting a possible effect originating from a nonzero surface desorption time.

Although the employed coating procedure was obtained after a thorough optimization study (described in [14]), it cannot be ruled out that the observed excess plate heights are also partly due to some microscopic heterogeneities in the density of the hydrophobic alkyl chains [24]. Measurements using X-ray photoelectron spectroscopy and atomic force microscopy, however, did not reveal any conclusive data on possible coating heterogeneities.

Modeling the adsorption–desorption band broadening

In the paragraph below, we have generalized the Giddings random-walk (RW) theory [10] to make it applicable in the specific geometry of shear-driven (SD) flow channels. The emphasis is on channels with a flat-rectangular cross-section, for this is the format that is most suited for SDC, but the general theory is applicable to any type of cross-sectional channel shape.

Establishment of a theoretical plate height expression

According to Giddings [10], the effect of a nonzero adsorption–desorption time can be accounted for by representing the sequence of adsorption–desorption processes as a RW process wherein the species can make different steps with respect to the mean species velocity.

In pressure-driven (PD) flows through open-tubular channels (Fig. 4a), molecules that are adsorbed on the coated wall either make a backward RW step with respect to the mean species velocity (when being adsorbed on the stationary phase) or a forward RW step (when being desorbed from the stationary phase and being carried along by mobile phase flow having a mean velocity u_m). In electro-driven (ED) flows, the

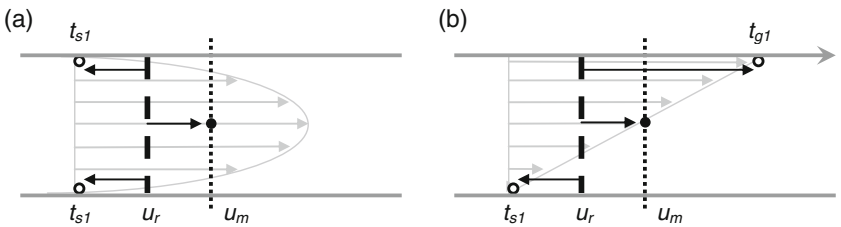

Fig. 4 Schematic overview of adsorption effects on the band broadening in open-tubular PD chromatography **(a)** and SDC **(b)** channel. The *bold dashed line* represents the average migration position of molecules having a mean retained velocity u_r, while the *dotted curve* represents the average migration position of a molecule traveling with the average mobile phase velocity u_m. The *open symbols* represent adsorbed molecules, while the *closed symbols* relate to a molecule in its desorbed state, during which it moves with an average velocity u_m. The *arrows* represent the different possible RW steps described in the text

velocity profile has a different shape, but the number and the length of the possible RW steps are identical to those for a PD flow.

In a shear-driven flow (Fig. 4b) on the other hand, where one wall is moving relative to the other one and wherein this moving wall should be left uncoated to avoid excessive dispersion, three basic steps should be considered. A backward step that is set by the molecules that are adsorbed on the stationary-phase coated wall, a forward step experienced when being dissolved in the mobile phase, and a second type of forward step while being adsorbed on the moving wall. As becomes readily apparent by comparing Figs. 4a, b, the SD flow system is intrinsically more prone to adsorption–desorption band broadening, for it contains an additional step that is inevitably larger (it goes outside the boundaries set by the u=0 and the u=u_m case) than the two step types that need to be considered in the case of an ED or PD flow.

Attempting now to quantify the band broadening that can be expected from the above-mentioned adsorption and desorption phenomena, a given step length ℓ_i should be associated to each of the different steps considered in Fig. 4. Focusing first on the SD case (Fig. 4b), it can be said that an analyte molecule will on the average stay at time t_c in the mobile phase once it is desorbed from a surface. During this time, it will migrate with an average velocity equaling that of the mobile phase velocity u_m and will hence travel a distance $\ell_c=t_c(u_m-u_r)$ with respect to the mean species velocity. This period is ended by an adsorption event on either the moving wall or the stationary wall. In the former case, the molecule will migrate at the moving wall velocity (which equals twice the mobile phase velocity in the case of an SD flow [25]) during a time t_{g1} and will hence make a step with length $\ell_{g1}=t_{g1}(2u_m-u_r)$ with respect to the mean species velocity. However, if the adsorption takes place on the stationary wall, the molecule will be immobilized (velocity=0) during a desorption time t_{s1}. In this case, the analyte will make a step backward with length $\ell_{s1}=-t_{s1}u_r$ with respect to the mean species velocity.

In summary, the three different steps that are made with respect to the position of the zone center of the peak (migrating through the channel at the retained velocity u_r) are given by:

$$\ell_c = (u_m - u_r)t_c \tag{7}$$

$$\ell_{g1} = (2u_m - u_r)t_{g1} \tag{8}$$

$$\ell_{s1} = (0 - u_r)t_{s1} \tag{9}$$

In general, the RW theory allows to demonstrate that the total molecule distribution variance σ^2_{tot} of a probabilistic process consisting of different independent subprocesses, each with a different step length and number of steps n_i, can be calculated using the following simple addition rule [10]:

$$\sigma^2_{tot} = \sum_i n_i \ell_i^2 \tag{10}$$

Denoting now the total number of adsorption events (either occurring on the moving wall or the stationary wall) by the number n and knowing that each period the molecule spends in the mobile phase is ended by an adsorption event, the number of steps in the mobile phase will also be equal to n. As the molecules have an equal probability to reach the moving wall or stationary wall, the number of adsorption events on each wall will be $n/2$. Considering then that the migrating species in the SD case can travel through the channel either by being transported by the mobile phase or while being adsorbed to the moving wall, the above also implies that the total migrated distance L is traveled by n steps in the mobile phase (velocity=u_m) and $n/2$ steps in the adsorbed state on the moving wall at the wall velocity (velocity=$2u_m$), yielding:

$$L = n \times t_c u_m + \frac{n}{2} \times 2t_{g1}u_m \tag{11}$$

The total number of adsorption events n can hence be written as a function of the migration distance L, the mobile phase velocity u_m, the adsorption time t_{g1} on the moving wall, and the mean time t_c a molecule spends in the mobile phase between successive desorption and adsorption events:

$$n = \frac{L}{u_m\left(t_c + t_{g1}\right)} \tag{12}$$

With the above, we can now rewrite Eq. 10 in a more explicit form:

$$\sigma^2_{ads,SD} = n\ell_c^2 + \frac{n}{2}\ell_{g1}^2 + \frac{n}{2}\ell_{s1}^2 \tag{13}$$

Subsequently using the relation between the mean species velocity u_r and the mobile phase velocity u_m given by Eq. 2 and using the experimentally determinable retention factor k' and introducing the result of Eqs. 7–9 and 12, Eq. 13 can be further transformed into:

$$\sigma^2_{ads,SD} = \frac{Lu_m}{\left(t_c + t_{g1}\right)(k'+1)^2} \times \left(k'^2 t_c^2 + \frac{(2k'+1)^2}{2}t_{g1}^2 + \frac{1}{2}t_{s1}^2\right) \tag{14}$$

Based on the definition of the plate height (Eq. 5), the additional band broadening due to adsorption–desorption effects in a shear-driven channel is hence given by:

$$H_{\mathrm{ads,SD}} = \frac{\sigma^2_{\mathrm{ads,SD}}}{L} = \frac{u_{\mathrm{m}}}{\left(t_{\mathrm{c}} + t_{\mathrm{g1}}\right)\left(k' + 1\right)^2} \times \left(k'^2 t_{\mathrm{c}}^2 + \frac{\left(2k' + 1\right)^2}{2} t_{\mathrm{g1}}^2 + \frac{1}{2} t_{\mathrm{s1}}^2\right) \tag{15}$$

Equation 15 still contains three unknowns (t_c, t_{g1}, t_{s1}), but it is possible to eliminate one of them by introducing the link between the observed retention factor and the mean single-event times t_c, t_{g1}, and t_{s1}. This can be achieved by noting that the retained velocity u_r equals the length of the chromatographic channel divided by the average residence time t_r of the molecules in that channel, which in turn can be split in three different fractions, one relating to each of the three different single-event times t_c, t_{g1}, and t_{s1}:

$$u_{\mathrm{r}} = \frac{L}{t_{\mathrm{r}}} = \frac{L}{n t_{\mathrm{c}} + \frac{n}{2} t_{\mathrm{g1}} + \frac{n}{2} t_{\mathrm{s1}}} \tag{16}$$

Combining now Eq. 16 with Eqs. 2 and 12, the values of t_c, t_{g1}, and t_{s1} are interdependent through the value of k':

$$k' = \frac{t_{\mathrm{s1}} - t_{\mathrm{g1}}}{2\left(t_{\mathrm{c}} + t_{\mathrm{g1}}\right)} \tag{17}$$

allowing to rewrite the adsorption plate height equation only as a function of t_c and t_{g1} :

$$H_{\mathrm{ads,SD}} = \frac{u_{\mathrm{m}}}{\left(t_{\mathrm{c}} + t_{\mathrm{g1}}\right)\left(k' + 1\right)^2} \times \left(3k'^2 t_{\mathrm{c}}^2 + \left(2k' + 1\right)^2 t_{\mathrm{g1}}^2 + 2k'\left(2k' + 1\right) t_{\mathrm{c}} t_{\mathrm{g1}}\right) \tag{18}$$

In open-tubular PD and ED chromatographic systems, all walls are coated with the same stationary phase monolayer. As a consequence, there is only one adsorption time left, i.e., the average time for a single adsorption stay on the stationary phase coating (t_{s1}). This also implies that t_{g1} and ℓ_{g1} should be put to zero everywhere in Eqs. 8 and 11–13, while the $n/2$ associated with the t_{s1} time should be replaced by a factor n because the number of stays in the mobile phase is in the ED and the PD case equal to the number of stays on the stationary phase. By applying these changes, Eqs. 15 and 17 transform into:

$$H_{\mathrm{ads,PD-ED}} = \frac{u_{\mathrm{m}}}{t_{\mathrm{c}}\left(k' + 1\right)^2}\left(k'^2 t_{\mathrm{c}}^2 + t_{\mathrm{s1}}^2\right) \tag{19}$$

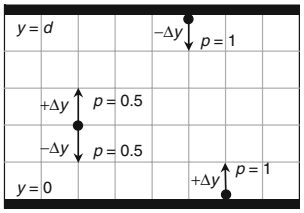

Fig. 5 Schematic representation of the random walk grid. After every time step Δt, the molecule (*black dot*) was allowed to travel a distance Δy in either positive or negative direction with a probability p of 0.5. At the surface, the molecule was forced to travel away from the surface (p=1) in the next time step

and:

$$k' = \frac{t_{\mathrm{s1}}}{t_{\mathrm{c}}} \tag{20}$$

such that one finally obtains:

$$H_{\mathrm{ads,PD-ED}} = 2\frac{k'}{\left(1 + k'\right)^2} u_{\mathrm{m}} t_{\mathrm{s1}} \tag{21}$$

which is equal to the original Giddings equation for PD flows (Eq. 3 with t_{s1}=t_d).

Determination of mean time t_c between two subsequent collisions with a wall

General expression for t_c derived from random walk simulations While Eq. 21 is relatively straightforward to use, the present SD case requires the use of Eq. 18, containing the additional unknown t_c. The latter is the time an analyte molecule spends in the mobile phase between successive desorption and adsorption events, or in other words, t_c is the average time between two successive collisions of a molecule with either channel wall. To arrive at an expression for this mean collision time, an extensive set of 1-D and 3-D random-walk simulations has been conducted using a self-written numerical routine in Fortran 90 code. In this routine, a molecule is released at a random position between two reflective walls ($0 \le y \le d$). As illustrated in Fig. 5, the molecule was allowed to travel a distance Δy in positive or negative direction at each time step Δt, with a probability of p=0.5 in either direction. The walls (y=0 and y=d) were made reflective by forcing the molecule to make a positive displacement Δy in case of y=0 and a negative displacement Δy in case of y=d. The travel time of a molecule between two successive collisions with any of the channel walls was recorded, and the average collision time was calculated from a large number of collisions.

Figure 6 shows an example of the obtained RW simulations, comparing two channels with a different depth d. A detailed look revealed that the time between two successive

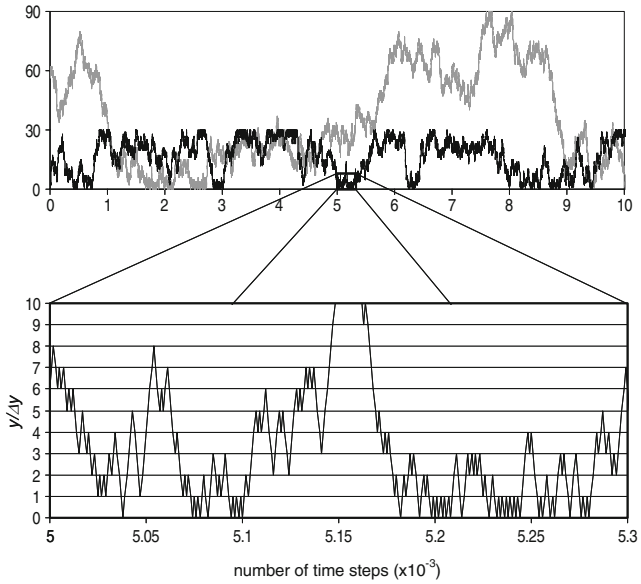

Fig. 6 Graph of the random walk trajectory of a molecule as function of time for two different channel heights, respectively, equal to 30 (*black curve*) and 90 (*dark gray curve*) times the displacement length Δy. The *zoom-in* reveals the high collision frequency with the same wall once a molecule gets into the vicinity of this wall

collisions (either with the same wall or with the opposite wall) doubles if the channel depth doubles.

Repeating the RW simulations for a wide variety of different values of Δt, Δy, and d, it was found that the average collision time in a channel with a flat-rectangular cross-section follows a perfectly linear relationship with the channel depth d, according to:

$$t_c = \frac{\Delta t}{\Delta y} d \quad \text{(1-D RW case)} \tag{22}$$

and

$$t_c = 3\frac{\Delta t}{\Delta y} d \quad \text{(3-D RW case)} \tag{23}$$

This linear dependency is quite surprising, for most phenomena related to diffusion events have a characteristic time that is proportional to the square of the distance. Nevertheless, the linear dependency is absolutely correct, for Eq. 22 can also be derived analytically, using the fundamental laws of probability theory. Doing so and following the theorems and rules in Chap. 14 in [26], one arrives exactly at Eq. 22. This independent control also proves that our numerical routine was error-free.

In fact, our simulations only yielded Eq. 22 with a proportionality constant equal to 1.00±0.02, but this should be attributed to the fact that the number of collision events that we took into account (typically some 50,000 events) was insufficiently high. Changing the number of collision events, the convergence trend clearly showed that the proportionality constant would converge closer to unity if more and more collisions would be taken into account.

In the case of a very thin channel, i.e., one wherein the radius R of the molecules, the extent δ_{ads} of the surface adsorption potential field or the height δ_r of the surface roughness would no longer be negligible compared to the rest of the channel, Eq. 22 should be corrected by subtracting these values from the actual channel depth. The 3-D version of Eq. 22 then becomes:

$$t_c = 3\frac{\Delta t}{\Delta y}(d - 2R - 2\delta_{max}) \tag{24}$$

with $\delta_{max}=\max(\delta_{ads}, \delta_r)$

The first correction (subtracting the quantity $2R$ from d) is needed because Eq. 23 has been established for a point-like object, whereas the analyte molecules of course have a finite size, preventing them to come closer to the wall surface than a distance equaling their radius. The factor 2 is used to account for the fact that this effect needs to be accounted for on both the top and the bottom surface. The second correction was introduced to express that molecules start to feel the attraction force of the adsorption potential field as soon as they reach a distance δ_{ads} from the surface or because the surface roughness creates stagnant pools of liquid (with depth δ_r) that make the liquid move along with the surface, such that (for what concerns its net migration velocity) a molecule that resides in these pools cannot be distinguished from a molecule that is actually adsorbed onto the wall. The presently proposed correction, i.e., simply subtracting the maximal value of δ_{ads} and δ_r, is certainly only a crude approximation and needs to be further refined depending on the actual topology of the surface, but such a detailed treatment is not needed for the remainder of the present study.

In fact, the net effect of the finite molecular size and the values of δ_{ads} and δ_r is that they make the channel less deep than its actual geometrical dimensions. It is as if the adsorption plane is displaced a given distance $R+\delta_{max}$ away from the actual wall surface.

Taking an even closer look at Fig. 6 (see inset), it can clearly be noted that the majority of the wall collisions occurs with the same wall. Most of the collisions counted during the RW simulations relate to desorption events wherein a molecule that has left the wall very rapidly returns to this same wall, while it only very rarely occurs that a molecule leaves one wall to experience a subsequent collision with the other wall. In fact, the probabilities of the RW system considered in Figs. 5 and 6 are such that one half of the total collision events relates to the case wherein the molecule just makes one upward jump (with step size=Δy) and then immediately returns back to the surface. It can even be

verified that about 90% of all wall collisions relate to desorption events wherein the molecules have not been further remote from the surface than ten displacement steps (data not shown). This number is independent of the actual channel height (provided the channel depth is much larger than Δy).

When the size of the molecule is much larger than the size of a single displacement Δy (and it actually is, see "Explicit expression for t_c using Langevin's theory" in "Determination of mean time t_c between two subsequent collisions with a wall"), those small jumps at the surface are actually nothing else but minor vibrations of the molecule along the surface. Since the present experimental approach (nor the other existing experimental approaches [19, 20, 21]) would allow to experimentally record desorption events that relate to a displacement that is only one tenth or less of the molecular size, one could opt to exclude these small local vibrations from the total number of wall collisions predicted by Eq. 24.

To make this possible, we repeated the RW simulations after having defined an adsorption zone with thickness y_{max} and only counted a collision if the molecule left this zone at least once before hitting the same wall again. The t_c values that were obtained with this assumption can be represented by the following approximate expression, holding very well for all cases wherein y_{max} is less than 5% of d:

$$t_c = 3\left(1 + \frac{y_{max}}{\Delta y}\right)\frac{\Delta t}{\Delta y}(d - 2R - 2\delta_{max}) \tag{25}$$

Although difficult to use in a straightforward manner (the value of y_{max} value has to be arbitrarily chosen), Eq. 25 can be used to exclude any desired type of small-scale molecular bumps from the number of wall collisions a given molecule can be expected to have. It is again also interesting to note that the exclusion of the very short intercollision distances still does not change the linear dependency between t_c and the channel depth.

Explicit expression for t_c using Langevin's theory Since the RW expressions in the previous paragraph depend on the arbitrary time and space steps Δt and Δy, the latter should first be related to the basic physico-chemical molecular parameters of the molecules before the RW expressions can be used to interpret any practical experiment.

A relation with the physico-chemical parameters can be established using Langevin's theory of Brownian motion [27]. It can be derived from Langevin's theory that the time t' during which a molecule can travel without colliding with another molecule corresponds to the time for which the equation of the particle motion switches from a constant linear motion (mean displacement $\sim t$) into a chaotic random walk (mean displacement $\sim\sqrt{t}$), with t' given by:

$$t' = \frac{2m}{\zeta} \tag{26}$$

Wherein m is the mass of the molecule (kg) and ζ is the friction coefficient (kg s^{-1}). For a spherical molecule, the friction coefficient is related to the viscosity μ (kg m^{-1} s^{-1}) and molecular radius R (m), as originally shown by Stokes [28]:

$$\zeta = 6\pi\mu R \tag{27}$$

Combining Eqs. 26 and 27, the inverse of t', corresponding to the intramolecular collision frequency ν, can hence be calculated to be:

$$\nu = \frac{1}{t'} = \frac{3\pi\mu R}{m} \tag{28}$$

Langevin's equation of particle motion also allows to relate the free path length λ of a molecule, i.e., the linear distance a molecule can travel without colliding another molecule, to this collision frequency, via:

$$\lambda = \sqrt{\frac{k_B T}{m}}\frac{1}{\nu} = \frac{\sqrt{k_B T m}}{3\pi\mu R} \tag{29}$$

Wherein k_B is the Boltzmann constant (kg m^2 K^{-1} s^{-1}), and T is the temperature (K).

To relate the results of the presently employed random walk model (cf. Fig. 5) to the physical reality, it suffices to equate the employed displacement step Δy to the free path length λ ($\Delta y = \lambda$) and to equate the time step Δt to the inverse of the collision frequency ν ($\Delta t = 1/\nu$).

These values of Δy and Δt are also related to the molecular diffusion coefficient D_M by the Einstein–Stokes equation [27]:

$$D_M = \frac{k_B T}{6\pi\mu R} = \frac{1}{2}\frac{\Delta y^2}{\Delta t} \tag{30}$$

In the present study, Eq. 30 was used to obtain a good estimate for the molecular radius R from the available D_M values.

Using typical values for μ(~1.7×10^{-3} kg m^{-1} s^{-1}), m (~3.5×10^{-25} kg), T (293 K) and D_M (3.5×10^{-10} m s^{-1}), it can be calculated from Eq. 30 that the radius of the molecule is about 0.35 nm, while the corresponding free path length or step size Δy is about 7×10^{-12} m and hence 50 times smaller than the molecular radius. The definition of a collision zone with a thickness of for example $y_{max} = 10\times\Delta y$ (see establishment of Eq. 25) as a means to eliminate small-scale molecular vibrations from the total number of wall collisions hence still correspond to a zone with a thickness equaling only one tenth of the molecular size.

Extraction of the mean adsorption–desorption times from the experimental data and their implication on the chromatographic performance of open-tubular nanochannels

Considering Fig. 3, the excess plate height values in the weak retention case (gray data points) is clearly insignificant. Trying to estimate surface desorption times form this data set was hence considered to be meaningless.

Turning now to the strong retention data (black data points), it should first be noted that, as already remarked in "Experimental observations," it cannot be ruled out that part of the observed excess plate height is due to some microscopic heterogeneities in the density of the hydrophobic alkyl chains. The presently obtained values for the surface desorption times (t_{g1} and t_{s1}) should therefore be considered as an upper limit rather than the true value.

Table 2 gives an overview of the obtained t_{g1} and t_{s1} values. These values were determined using the solver function of Excel to yield a best fit value for the glass wall desorption time t_{g1} by fitting Eq. 18 onto the experimental data. The value of t_{s1} was subsequently calculated from Eq. 17 using the k' value that was derived from the observed peak velocity and the mean mobile phase velocity using Eq. 2. Under the applied strong retention conditions (50:50% (v/v) MeOH/H_2O), the desorption times of the coumarine molecules could be calculated to vary between 60 and 150 μs on the uncoated moving fused-silica glass wall (t_{g1}), while they are of the order of 100 to 500 μs on the hydrophobically coated stationary wall (t_{s1}). The differences in surface chemistry hence clearly influence the desorption time.

The values for t_c in Table 2 were directly obtained from Eq. 23, using the nominal channel depth as the value for d. Corrections for $2R$ and δ_{max} (determined for a surface roughness of 3.5 nm as measured with a noncontact optical profiler) only reduced the value of t_c with 3.5%. This change had no significant effect on the values for t_{g1} and t_{s1}.

The data in Table 2 also show that, in the presently investigated case, the time the analytes spend on the surface of the naked glass wall or on the monolayer coated wall is orders of magnitude larger than the mean time in between two collisions. With $t_c \ll t_{g1}$, this also implies (see Eq. 11) that the analytes essentially move forward through the channel by being adsorbed to the moving top wall, rather than by being transported by the mobile phase flow. The fact that $t_c \ll t_{g1}$ also explains why a change in adopted t_c value has so little impact on the t_{g1} time derived from Eq. 18.

If desired, one could also decide to eliminate the small submolecular scale bumps a molecule can make during its random walk close to a surface from the total number of desorption events. This can be accomplished using Eq. 25, although we can only make a very crude estimate for y_{max}. Assuming that a molecule needs to be at least one molecular diameter away from the surface or the adsorption potential field before it can really be considered as being detached, it seems a plausible guess to take y_{max} equal to the size of one molecular diameter, which, in the present case, is equal to about 0.6 nm. Although this correction increases t_c 30-fold, the effect on t_{g1} and t_{s1} still remains very small (less than 0.8%), again because still $t_c \ll t_{g1}$.

Turning now to the intrinsic difference between SD flows on one hand and PD and ED flows on the other hand (cf. the discussion of Fig. 4), a separation with the same k' value as in the presently investigated strong retention case but performed using a PD flow is considered. For this fictive PD case, the values of t_c will be nearly identical to the SD case because they only depend on the physicochemical parameters of the molecules and the channel depth d, i.e., parameters which mainly remain constant. The values of the desorption times t_{s1} however will differ strongly from the SD case as they are directly related to the values of t_c and k' by Eq. 20. By adapting these t_{s1} values to obtain the same k' factor, it is found that the contribution of H_{ads} in the PD case would be about 6,000 times smaller than in the SD case at a typical mobile phase velocity of 2 mm/s. This remark now quantifies the statement that SD flows are intrinsically much more prone to the effect of nonzero adsorption–desorption times.

Conclusion

Nanochannel separations are very sensitive to wall adsorption effects. Depending on the mobile phase, the residence time per collision can vary strongly. The present study has indicated that shear-driven flows are intrinsically much

Table 2 Employed physicochemical parameters and experimentally obtained values for t_{g1} and t_{s1} under strong retention conditions

	μ ($\times 10^{-3}$ kg m^{-1} s^{-1})	m ($\times 10^{-25}$ kg)	D_M ($\times 10^{-10}$ m^2 s^{-1})	R (nm)	Δt ($\times 10^{-14}$ s)	Δy ($\times 10^{-12}$ m)	t_c (ns)	t_{g1} (μs)	t_{s1} (μs)	k'
C450	1.77	3.60	3.5	0.35	6.23	6.37	3.40	60	95	0.29
C460	1.77	3.83	3.2	0.38	6.05	6.01	3.63	112	265	0.69
C480	1.77	4.23	3.1	0.39	6.50	6.11	3.81	147	482	1.10

more prone to nonzero adsorption–desorption times than pressure- and electro-driven flows (unless the adsorption to the moving wall needed to generate SD flows could be completely blocked). This limits the range of application of SD flows to conduct chromatographic separations but opens up a new application field, i.e., SD flows could be used as a tool to measure wall adsorption–desorption times in a systematic way, for a broad variety of liquids, wall surfaces, and analytes (as long as they can be visualized by fluorescence microscopy).

Albeit subject to a number of assumptions (obtained desorption times should be regarded as upper limits), the present study showed that the surface desorption times on naked fused-silica glass are maximally of the order of some 60 to 150 μs, while they are maximally on the order of 100 to 500 μs when these walls are hydrophobically coated (cited values are for a coumarin dye analyte dissolved in 50:50% (*v*/*v*) methanol/water mixtures buffered at pH 3 and tested in 120 nm deep channels).

To interpret the experimental data, a series of random-walk simulations has been conducted, allowing to establish explicit expressions allowing to relate the time between two successive wall collisions to the fundamental parameters (persistence length and intramolecular collision frequency) determining the diffusion rate in a liquid. Whereas the basic expression (Eq. 22) can also be directly derived from the probability theory (ruin games theory [26]), the presently proposed RW study has extended this expression to account for the finite size of the molecules, the effect of thickness of the surface adsorption potential field, and the surface roughness. In addition, an expression has been established that allows to eliminate small molecular vibrations from the total number of wall collisions.

Symbol list:

C_m	Mass transfer resistance in the mobile phase (s)
D_M	Molecular diffusion coefficient ($m^2\ s^{-1}$)
H	Plate height value (m)
H_{theo}	Theoretical plate height value (m)
H_{meas}	Measured plate height value (m)
$H_{ads,PD\text{-}ED}$	Plate height due to adsorption/desorption effects in case of a PD and ED flow (m)
$H_{ads,SD}$	Plate height due to adsorption/desorption effects in case of a SD flow (m)
δ_{ads}	Height over which the adsorption potential field is felt by the analytes (m)
δ_r	Height of stagnant fluid zone caused by surface roughness (m)
δ_{max}	Max(δ_{ads}, δ_r) (m)
d	Channel depth (m)
Δt	Time step in RW model (s)
Δy	Step length in RW model (m)
k_B	Boltzmann constant ($1.3806503 \times 10^{-23}\ m^2\ kg\ s^{-2}\ K^{-1}$)
k'	Retention factor (/)
λ	Free path of a molecule (m)
ℓ_i	Molecular RW step length relative to the mean species velocity with $i=c$ in the mobile phase; $i=$ g1 when adsorbed on the moving wall or $i=$s1 when adsorbed on the stationary wall (m)
L	Travel distance (m)
L_0	Travel distance of an unretained peak (m)
L_{eff}	Travel distance of a retained peak (m)
m	Mass of the analyte (kg)
μ	Dynamic viscosity ($kg\ m^{-1}\ s^{-1}$)
n	Number of adsorption events (/)
ν	Intermolecular collision frequency (s^{-1})
R	Radius of the analyte (m)
t	Time (s)
t_c	Time between two successive collisions with a wall (s)
t_d	Desorption time (s)
t_{g1}	Desorption time on moving wall (s)
t_{s1}	Desorption time on stationary wall (s)
t'	Time between two successive intermolecule collisions (s)
T	Temperature (K)
u	Fluid velocity ($m\ s^{-1}$)
u_m	Mean mobile phase velocity ($m\ s^{-1}$)
u_r	Mean species velocity ($m\ s^{-1}$)
σ^2	Peak variance (m^2)
$\sigma^2_{ads,PD\text{-}ED}$	Peak variance due to adsorption/desorption effects in case of a PD or ED flow (m^2)
$\sigma^2_{ads,SD}$	Peak variance due to adsorption/desorption effects in case of a SD flow (m^2)
w_{inj}	Injection peak width (m)
y_{max}	Thickness of the adsorption zone (m)
ζ	Friction coefficient ($kg\ s^{-1}$)

Acknowledgments F.D. gratefully acknowledges a research grant from the Research Foundation-Flanders (FWO Vlaanderen).

References

1. Harrison DJ, Fluri K, Effenhauser CS, Manz A (1993) Science 261:895–897
2. Gavin PF, Ewing AG (1997) Anal Chem 69:3838–3845
3. Cao H, Yu ZN, Wang J, Tegenfeldt JO, Austin RH, Chen E, Wu W, Chou SY (2002) Appl Phys Lett 81, 1:174–176
4. TegenFeldt JO, Prinz C, Cao H, Huang RL, Austin RH, Chou SY, Cox EC, Sturm JC (2004) Anal Bioanal Chem 378:1678–1692

5. Eijkel JCT, van de Berg A (2005) Microfluid Nanofluid 1:249–267
6. Janasek D, Franzke J, Manz A (2006) Nature 442:374–380
7. Eijkel JCT, van den Berg A (2006) Electrophoresis 27:677–685
8. Nichols KP, Eijkel JCT, Gardeniers JGE (2008) Lab On a Chip 8:173–175
9. Somorjai GA (1994) Introduction to surface chemistry and catalysis. Wiley, New York
10. Giddings JC (1965) Dynamics of chromatography. Marcel Dekker, New York
11. Clicq D, Vervoort N, Vounckx R, Ottevaere H, Buijs J, Gooijer C, Ariese F, Baron GV, Desmet G (2002) J Chromatogr A 979:33–42
12. Clicq D, Vankrunkelsven S, Ranson W, De Tandt C, Baron GV, Desmet G (2004) Anal Chim Acta 507:79–86
13. Vankrunkelsven S, Clicq D, Cabooter D, De Malsche W, Gardeniers JGE, Desmet G (2006) J Chromatogr A 1102:96–103
14. Fekete V, Clicq D, De Malsche W, Gardeniers JGE, Desmet G (2007) J Chromatogr A 1149:2–11
15. Fekete V, Clicq D, De Malsche W, Gardeniers JGE, Desmet G (2008) J Chromatogr A 1189:2–9
16. Neue UD (1997) HPLC columns: theory, technology and practice. Wiley, New York
17. Poppe H (1997) J Chromatogr A 778:3–21
18. Wirth MJ (2007) J Chromatogr A 1148:128–130
19. Swinton DJ, Wirth MJ (1998) Anal Chem 70:5264–5271
20. Wirth MJ, Ludes MD, Swinton DJ (1999) Anal Chem 71:3911–3917
21. Ludes MD, Anthony SR, Wirth MJ (2003) Anal Chem 75:3073–3078
22. Carr PW, Li J (1997) Anal Chem 69:2530–2536
23. Poppe H (1992) Chromatography, fundamentals and applicatons of chromatography and related differential migration methods. In: Heftmann E (ed) Journal of Chromatography Library. Elsevier, Amsterdam, pp 151–225
24. Gritti F, Guiochon G (2005) Anal Chem 77:1020–1030
25. Desmet G, Baron GV (1999) J Chromatogr A 855:57–70
26. Feller W (1968) An introduction to probability theory and its applications. Wiley, London
27. Berry RS, Rice ST, Ross J (1980) Physical chemistry. Wiley, New York
28. Atkins PW (1990) Physical chemistry fourth edition. Oxford University Press, Oxford
29. Giddings JC (1961) J Chromatogr 5:46–60
30. Jorgenson JW, Lukacs KD (1981) Anal Chem 53:1298–1302
31. Poppe H (2002) J Chromatogr A 948:3–17